Obliquely backscattered Thomson scattering system on the compact helical system

K. Narihara, T. Minami, I. Yamada, and K. Yamauchi
National Institute for Fusion Science, Nagoya 464-01, Japan

(Received 14 April 1995; accepted for publication 23 May 1995)

A Thomson scattering system with an obliquely backscattered configuration with a novel, high throughput collection system was developed and tested on a plasma confinement device, the compact helical system. It can yield the full profiles of electron temperature and density along a major radius with the spatial resolution ranging from 1.5 to 4 cm at a repetition rate of up to 250 Hz. © *1995 American Institute of Physics.*

I. INTRODUCTION

A Thomson scattering (TS) system which can give full profiles of electron temperature, T_e, and density, n_e, along a major radius of a toroidal plasma is very attractive, as demonstrated by the TV Thomson on TFTR[1] and by the LIDAR on JET,[2] in that it yields the shift and deformation of nested magnetic flux tubes in addition to the electron heat and particle transport coefficients. Such a TS system is realized by using light collection optics (a lens or mirror system) which can view a long distance along the laser beam passing along a major radial vector on the midplane. In addition to this wide angle capability, the light collection optics is required to have a large solid angle ($>10^{-2}$ sr) to obtain high quality data with the presently available lasers and light detectors. In designing such an optical system we often encounter difficulties caused by the port configuration of a plasma confinement device. This is particularly the case for stellarators, in which helically wound coils limit the space for necessary ports; and for the next generation tokamaks (e.g., ITER), which are equipped with only small ports for diagnostics. In this regard, LIDAR is the best choice, because its backscattering nature allows a long distance observation through light collection windows which are located very close to the laser injection window. Regrettably, its poor spatiotemporal resolutions make the present LIDAR less attractive for the contemporary fusion oriented plasma experiments, in which measuring the profile evolution is highly important. Then a natural question arises: what about adopting this backscattering configuration for a conventional TS system? Apparently, as the scattering angle approaches 180°, the viewing distance will become longer but the spatial resolution will become worse. Then some trade-off between the length of the observation and the spatial resolution is required. (For LIDAR the spatial resolution on the image is almost completely lost, but it is recovered by the time resolution through the light-cone condition.) Moreover, the fact that the image of a laser beam is heavily inclined or even curved will make the collection optics complex. We have examined the feasibility of this backscattering configuration for the large helical device[3] (LHD), now under construction at the National Institute for Fusion Science, and have concluded[4] that, by adopting advanced components such as low divergence lasers and optical fibers with large core diameter, we will attain reasonable performance (spatial resolution $\Delta x=2.0$–4.0 cm for the entire observation length of 200 cm). Before actually installing this TS system on LHD, we designed and constructed a prototype for the compact helical system (CHS),[5] which is also a pilot machine for the LHD, to check the overall performance of the system. This is of great importance because the proximity between the plasma and the laser exit tube in the viewing scope may introduce an unexpectedly large amount of stray light, thereupon deteriorating the data quality appreciably. This paper describes the design and performance of this TS system.

II. DESCRIPTION OF THE SYSTEM

Basically our design followed the so-called "YAG-Thomson" first developed by the ASDEX group,[6] because it today gives the best performance in terms of the spatiotemporal resolutions.

A. CHS vacuum chamber

Figure 1 shows the top and side views of CHS.[5] It is equipped with two helically wound coils and has a symmetry of the rotation group C_8. The vacuum chamber is a torus formed by rotating an ellipse (80 cm major diameter × 38 cm minor diameter) in the same way as the coils with its center being fixed at the major radius $R=100$ cm and the vertical coordinate $Z=0$ cm. Several kinds of ports are bored on the vacuum chamber, of which the outer and inner midplane ports are used for the TS system.

B. Laser beam optics

For a repetition rate of 250 Hz, the laser beams from five Nd:YAG lasers (Continuum NY81-50C: repetition of 50 Hz, pulse energy 0.55 J, beam divergence 0.5 mr, pointing stability 0.15 mr, beam diameter 9 mm, pulse width 8 ns) are "packed" so that they pass nearly a common path in the CHS vacuum chamber. The mirror system (Fig. 2) for this "beam packing" is a development from that first installed on Doublet-III.[7] Each bending mirror, a 14 mm × 20 mm ellipse, is formed on an antireflection coated BK7 glass of 80 mm in diameter, which allows the upstream laser beams to pass very near the mirror. Each glass being mounted on a precise gimbal-type holder, the mirror direction is precisely adjusted and very firmly kept. The beam–beam separation of the packed beam is 14 mm. After traveling a distance of 20

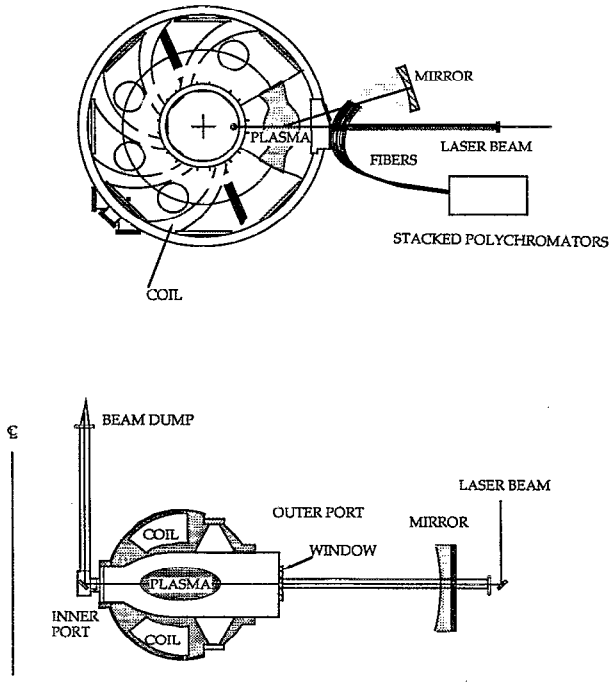

FIG. 1. Top and side views of the CHS equipped with the Thomson scattering system.

m by means of multiple reflections, the laser beams are focused by an $f=3$ m lens to give the scattering volumes shown in Fig. 3. The focal length, the position of the lens, and the tilting angles of the five beam-packing mirrors are optimized to give the smallest scattering volumes along a major radius on the midplane in the plasma. To keep the beam dump, which is the brightest source of stray light, away from the view scope, the laser beams are reflected upwards at the outside of the inner port by a metallic mirror with high reflectance (>98%) and directed to a beam dump made of carbon plates through a 2-m-long tube. Several light baffles are set inside the entrance and exit tubes to trap stray light.

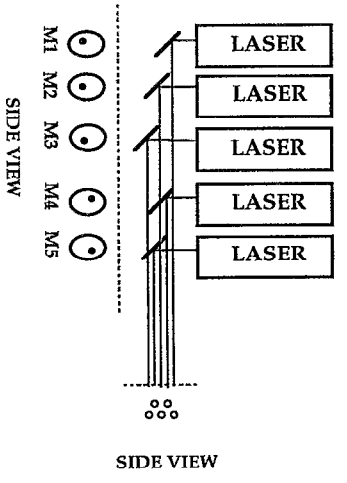

FIG. 2. Optical setup for packing five laser beams.

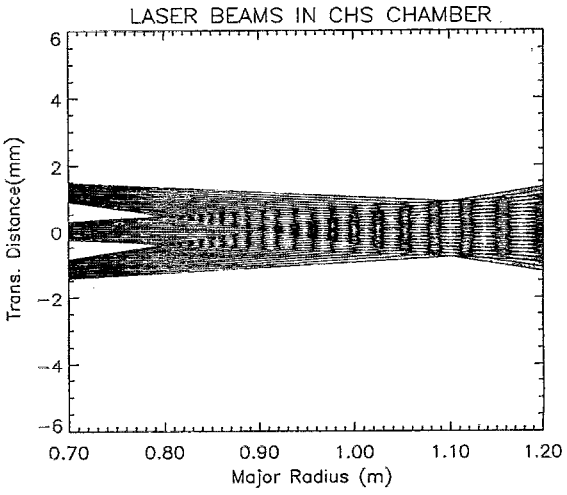

FIG. 3. Envelope of laser beams in the CHS chamber.

C. Light collection optics

The light collection optics was designed so as to optimize both the spatial resolution and light collection efficiency under the given port configuration. A collection window of 0.2 m in diameter is attached to the same outer port with the maximum allowed center to the laser beam separation of 0.2 m at the major radius $R=1.6$ m. The window is protected against thin film deposition during cleaning discharges by shutters. A gold-coated spherical mirror ($D_c=0.5$ m diam and $R_c=1.018$ m the radius of curvature) is set so that its center of curvature is located on the center of the collection window. Since most of the collected light passes near the center of the sphere, all the aberrations except the spherical one are kept to a minimum level. The diameter of the circle of least confusion for the spherical aberration is easily calculated as

$$D_{\mathrm{DLC}}=(R_c/32)(D_C/R_C)^3(1-m)^2/(1+m),$$

where m is the magnification. The dependence of D_{DLC} on the position of the scattering volume R is plotted in Fig. 4(a) together with the magnification [Fig. 4(b)]. Since the object (the laser beam) is inclined with respect to the optical axis, the image is also inclined and somewhat curved. The angle between the image of the laser beam and the optical axis is plotted in Fig. 4(c).

D. Fiber optics

Optical fibers are necessary for transporting the light collected along the inclined image to the entrance of polychromators efficiently. The laser beam size, the magnification, and the diameter of the circle of least confusion require the fiber to have a diameter larger than 2 mm. To accept a large fraction of light reflected by the mirror, the fiber needs to have a numerical aperture (NA) larger than 0.3. The optical fibers of these specifications are usually fabricated by bundling fine fibers (e.g., 200 μm core diameter), but the transmission is limited below 70% due to a finite packing fraction. To avoid this unnecessary loss, we have had fabricated single fibers of this size (fused silica core of 2 mm in diam-

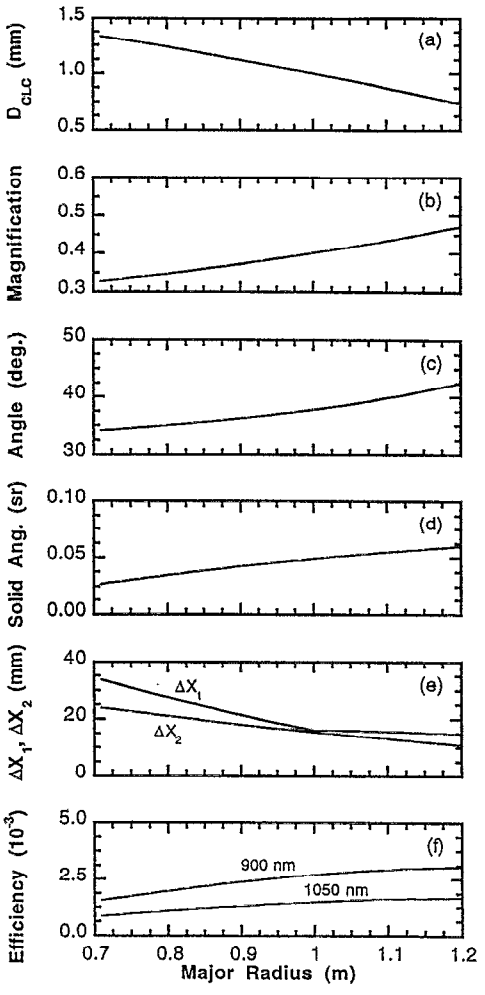

FIG. 4. Scattering position dependence of (a) the diameter of the circle of least confusion (D_{CLC}), (b) magnification (m), (c) the angle between the image and the optical axis, (d) the effective solid angle, (e) the separation between successive scattering volumes $\Delta X1$ and the extent of the scattering volume which a fiber can see, $\Delta X2$, (f) the overall light detection efficiency for λ=900 nm and λ=1050 nm.

eter, polymer clad of 2.1 mm in diameter, nylon jacket of 3 mm in diameter, and NA=0.33). The tips of the arrayed fibers are cut at 55° to avoid the blocking due to the otherwise neighboring fibers (Fig. 5). At first glance this heavily inclined image may seem to cause a large reflection at the

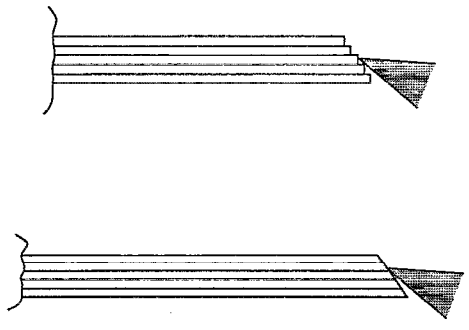

FIG. 5. Coupling of the collected light onto the tip of normally and obliquely cut fibers.

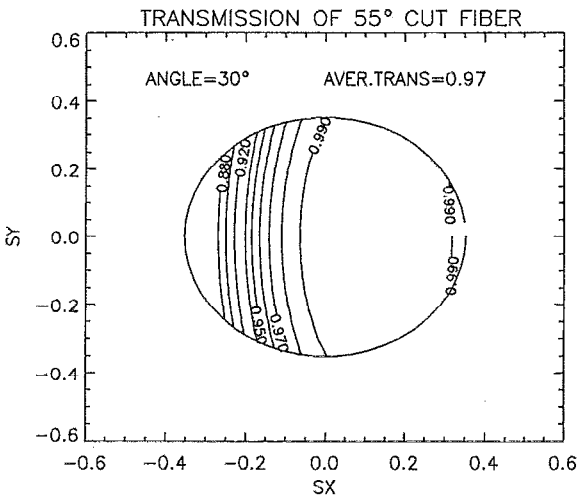

FIG. 6. Contour map of the transmission at the tip of the fiber as a function of the x and y components of the incident vector.

surface of the fiber tips, but it is avoided by using a laser beam which is horizontally polarized in the plasma. By taking into account the polarization of the scattered light and the change of it at the mirror surface, the transmission at the fiber tip is calculated as a function of the x and y components of the incident vector and is contour mapped in Fig. 6. The average transmission is 97% for a 30° inclined image, which is higher than the normal incidence transmission of 96%. The range of the direction of scattered light which is reflected by the mirror and then finally admitted by the fiber (solid angle) is somewhat complicated due to the finite size of mirror, the NA of the obliquely cut fibers, and the presence of the array of fibers in the scope of the mirror. The arrayed fibers and support structure are arranged so that their cross section seen from points on the midplane is at a minimum. The reduction of the solid angle due to the presence of the fibers is less than 10%. The solid angle thus considered is plotted in Fig. 4(d) as a function of the scattering position.

E. Polychromators

A conventional filter polychromator design was adopted because it accepts light from fibers with a large NA and offers a high transmission. To reduce cost, the number of filters is limited to three, which reduces the dynamical range of the T_e measurement and the confidence. This filter number is the minimum necessary both to deduce (T_e,n_e) and to check the validity of the assumption that the velocity distribution of plasma electrons is Maxwellian. A properly chosen three-filter combination can discriminate T_e over an order of magnitude, which is large enough for fixed-point measurements but is not enough for a whole profile measurement. To cover the whole T_e profile, we prepared four different filter combinations which cover T_e ranging 2.5–20, 7–50, 20–400, and 40–2000 eV, respectively, and distributed in accordance with the expected T_e profile. The filters transmit >70%–80% of an incident light in passbands and reflect >95% outside the bands; these give, together with the reflectance losses at the surfaces of lenses (4%), an overall throughput larger than 66%. In order to operate in an intense

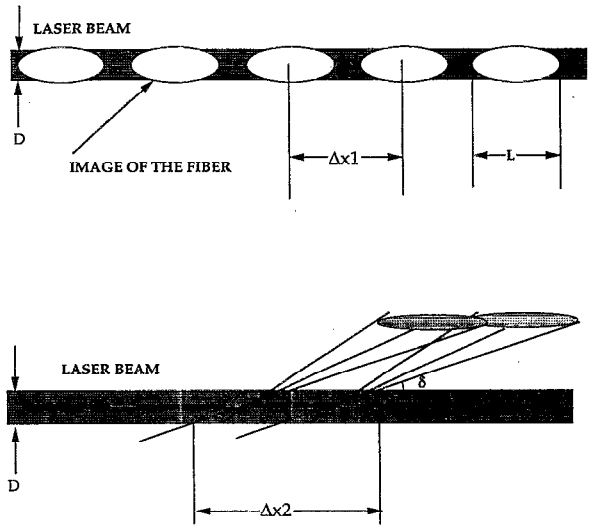

FIG. 7. A drawing explaining the spatial resolution.

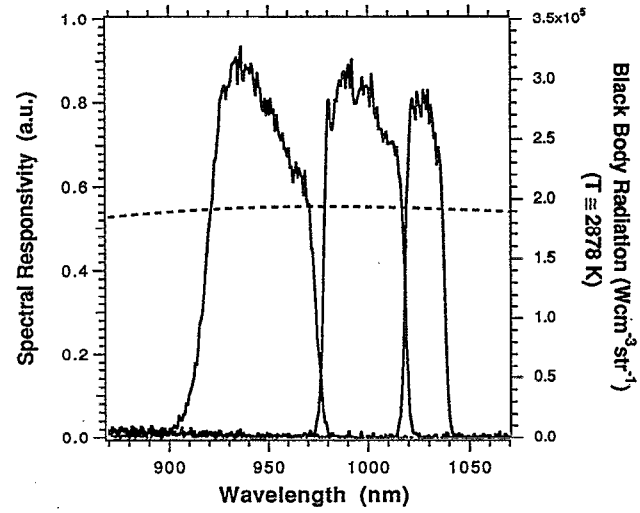

FIG. 8. The three channel spectral responsivities for a polychromator. Overplotted is the spectrum of the 2878 K blackbody radiation.

stray light, each filter was specified to have a high rejection power ($>10^5$) at the laser wavelength (1064 nm).

The requirements for detectors are: a high quantum efficiency, a wide bandwidth, a large sensitive area, and a wide acceptance angle. These are satisfied by the avalanche photodiode C30950E-956E (EG&G Canada) with an internal preamplifier. The specifications are as follows. The quantum efficiency is 80% at 900 nm and 40% at 1060 nm; the bandwidth is 25 MHz; the sensitive size is 3 mm in diameter, and the full acceptance angle is 104°.

F. Spatial resolution

To define the spatial resolution, two characteristic lengths should be considered: one is the separation between successive scattering volumes $\Delta X1$; and the other is the extent of the scattering volume which a fiber can "see", $\Delta X2$. These are schematically depicted in Fig. 7. Apparently, $\Delta X2$ grows rapidly as the scattering angle approaches 180° or as the laser beam size becomes larger. In Fig. 4(e), $\Delta X1$ and $\Delta X2$ are plotted as functions of the scattering position. Here, we define the spatial resolutions as the larger of $\Delta X1$ and $\Delta X2$. It is noted that better spatial resolution is obtained for the outer edge region, where the gradients of T_e and n_e are steepest.

G. Overall light detection efficiency

The efficiency of detecting photons scattered at a scattering volume is the product of the following factors: (1) the integration of the differential scattering cross section over the solid angle divided by that over the entire angles (4π), (2) the transmission of the uncoated window ~92%, (3) the reflectance of the Au-coated mirror ~0.98 for the wavelength range 700–1100 nm, (4) the coupling of the collected light onto the tip of the fibers, which is slightly less than unity due to the aberration and finite size of the laser image, ~0.97, (5) transmission of the fibers including the reflectance loss at both ends >0.93, (6) the transmission of the polychromators >0.66, (7) the quantum efficiency of the detectors: ~0.8 at 900 nm and ~45% at 1050 nm. The last two depend on the wavelength. The overall light detection efficiency is shown in Fig. 4(e) as a function of the major radius for two different wavelengths.

III. CALIBRATION

The spectral responsivities of three channels on each polychromator were measured by use of a standard-lamp–monochromator combination whose output was calibrated by a power meter (Yokogawa 3292) with a 4% uncertainty in the absolute sensitivity. An example is shown in Fig. 8 together with the spectral of the blackbody radiation from a 2878 K filament. The overall consistency was checked by feeding this blackbody radiation directly to the entrance of polychromator: the expected signal ratio is $x:y:z$ =2.57:2.14:1, while the measured ratio is $x:y:z$ =2.50:2.07:1, which demonstrates a good overall consistency within a 3.5% error. Raman scattering of a YAG laser by hydrogen molecules was used for the absolute calibration.

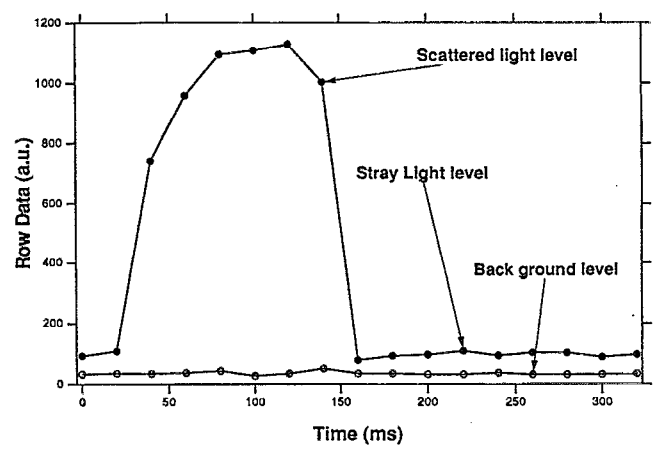

FIG. 9. Raw data from an inner channel where the stray light level is at a high level.

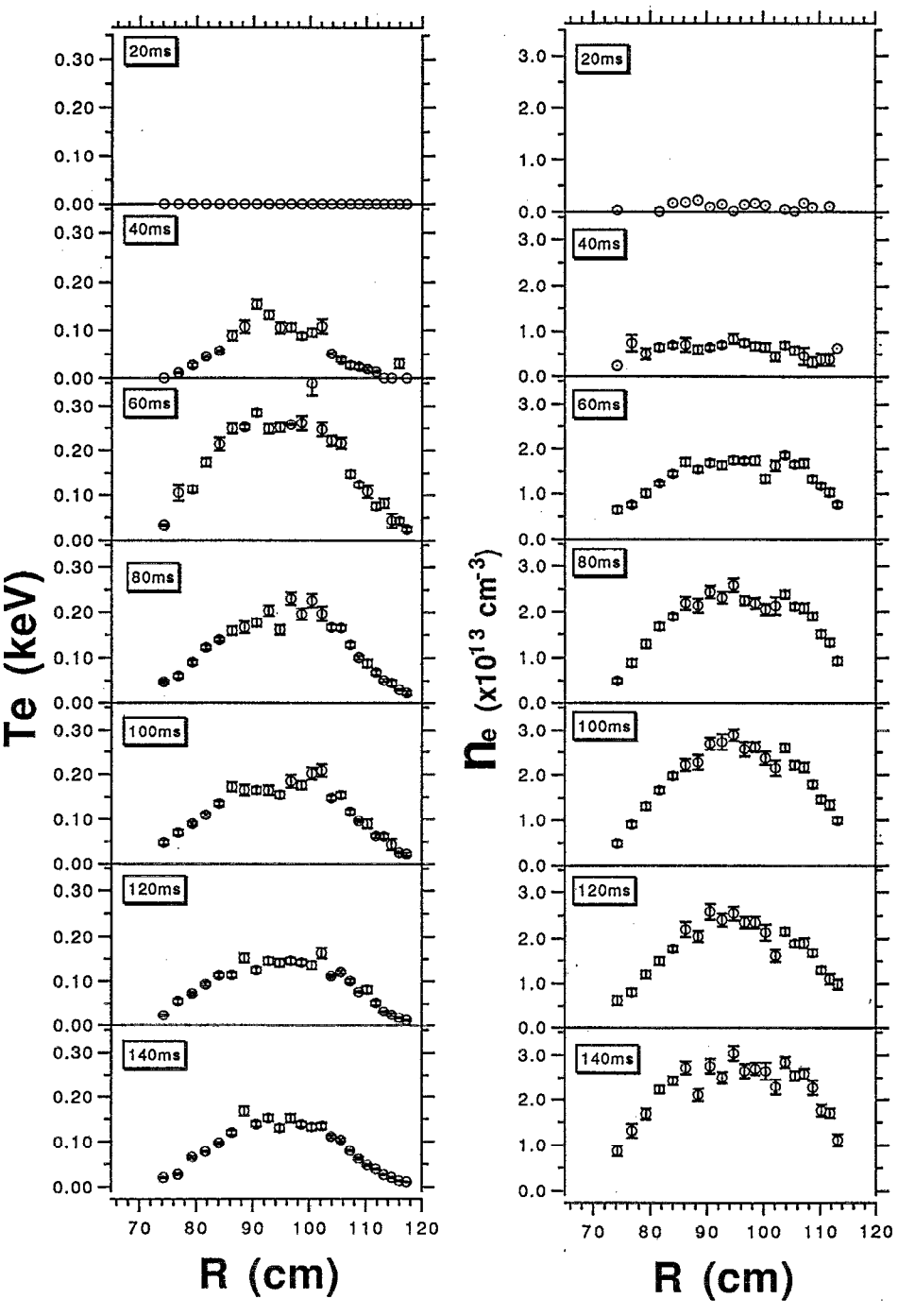

FIG. 10. Examples of the snapshot of T_e and n_e profiles.

Though this procedure is conventional, the difference in the angular dependence of the Raman and Thomson scattering cross sections needs some corrections for each scattering position.

IV. PERFORMANCE

First, the 72 raw signals from 24 polychromators were carefully examined. For most channels, the level of stray light is less than 4% of the scattering signal from $n_e = 1 \times 10^{13}$ cm^{-3} plasma. For three channels which see the inner parts of plasma, however, the stray light level exceeds 8% of the scattering signals (Fig. 9). The stray light level fluctuates pulse by pulse, probably due to the shift of laser beam position, introducing errors in the deduced T_e and n_e. The background level, plasma light plus circuit noise, is well below the signal level. Sequences of snapshots of T_e and n_e profiles for a typical plasma discharge are shown in Fig. 10. The T_e at the outer edge region was measured with a sufficient accuracy down to 10 eV. Occasionally, some irregularities appear in the T_e and n_e profiles in the central region of

the plasma. In spite of repeated careful calibrations of the responsivities, these could not be removed. The causes of these irregularities are now under investigation.

V. DISCUSSION

It seems that the level of performance demonstrated on CHS will be realized easily on LHD, but differences between the CHS and LHD port configurations necessitate some considerations. The larger aspect ratio, length/diameter, of the LHD outer port requires the scattering angles be closer to 180°, which, in turn, needs smaller magnification to keep the inclination of the image below a certain level above which the reflection at the fiber tips grows largely. The enhanced spherical aberration due to the decreased magnification should be compensated for by lowering the maximum incident angle to the mirror. By the above reasoning, the effective solid angle for the central measurement is limited below 20 msr for the LHD, which is still large enough to obtain high quality data. For the same reason, the spatial resolution gets worse by several tens of %. On the other hand, wider space in the inner port region will relax the stray light problem.

ACKNOWLEDGMENTS

We are grateful to Dr. Y. Hamada and Dr. K. Matsuoka for their encouragement, and to C. Takahashi for his support in data acquisition.

[1] D. Johnson, N. Bretz, D. Dimock, B. Grek, D. Long, R. Palladino, and E. Tolnos, Rev. Sci. Instrum. **57**, 1856 (1986).

[2] H. Salzmann *et al.*, Rev. Sci. Instrum. **59**, 1451 (1988).

[3] A. Iiyoshi, M. Fujiwara, O. Motojima, and K. Yamazaki, Fusion Technol. **17**, 169 (1990).

[4] K. Narihara, I. Yamada, and T. Minami, in Proceedings of the Sixth International Symposium on Laser-Aided Plasma Diagnostics, Bar Harbor, ME, 1993 (unpublished), p. 108.

[5] K. Matsuoka *et al.*, in *Plasma Physics and Controlled Nuclear Fusion Research, Nice, 1988* (IAEA Vienna 1989), Vol. II, p. 411.

[6] H. Röhr and K.-H. G. Schramm, Nucl. Fusion **22**, 1099 (1982).

[7] P. K. Trost, T. N. Carlstrom, J. C. Deboo, C. M. Greenfield, C. L. Hsieh, and R. T. Snider, Rev. Sci. Instrum. **61**, 2864 (1990).